An Efficient Deep Learning-based Spectrum Awareness Approach for Vehicular Communication

Basit A. Zaidi[†], Mahmoud A. Shawky[†], Ahmad Taha[†], Qammer H. Abbasi[†],
Muhammad Ali Imran[†], and Shuja Ansari[†]
[†]James Watt School of Engineering, University of Glasgow, Glasgow, G12 8QQ, United Kingdom
Email: {s.zaidi.2, m.shawky.1}@research.gla.ac.uk,
{Qammer.Abbasi, Muhammad.Imran, Ahmad.Taha, Shuja.Ansari}@glasgow.ac.uk

Abstract—**Intelligent transportation systems require a reliable exchange of information between network terminals in different vehicular communication environments. Making effective use of the dedicated spectrum is crucial to maximizing communication performance. This requires optimising the modulation order according to different channel conditions. This paper proposes a lightweight spectrum awareness methodology that uses wideband spectrum monitoring and deep learning-based modulation classification techniques to optimise the modulation order. We introduce a channel quality indicator block in which the classifier's accuracy of detection is used as a forward indicator for the choice of the best modulation type for transmission. By using a 3D stochastic vehicular channel, we evaluate the classification performance at different channel parameter settings, including, speed, variance, and signal-to-noise ratio in urban and rural areas. The experimental analyses demonstrate the capability of the proposed approach to supporting a high detection probability for acceptable false decision-making $\leq 20\%$.**

Index Terms—**Deep learning, Modulation classification, Spectrum monitoring, Vehicular communication.**

I. INTRODUCTION

The adoption of intelligent transportation systems contributes to decreasing the number of road fatalities and improving transportation safety [1]. By allowing wireless communication between different vehicular ad-hoc network (VANET) terminals, traffic-related messages are shared among vehicles [2]. These messages include critical traffic information such as location, speed, heading, etc. VANET is a mobile communication technology used in the vehicle domain that facilitates vehicle-to-vehicle (V2V) and vehicle-to-infrastructure (V2I) communications [1], [2]. Due to the recent influx of wireless technologies, the dedicated short-range communication (DSRC) spectrum (5.85 to 5.925 GHz) becomes fully occupied, limiting the communication throughput, especially in traffic congestion scenarios. This matter motivated researchers to turn to the unoccupied frequency spectrum to increase the network capacity [3]. Optimising communication performance in VANET requires terminals to have a good observation of the channel spectrum, referred to as "spectrum awareness." In general, spectrum awareness includes interference environment identification and modulation classification [4]. Accordingly, it is imperative to implement reliable spectrum monitoring techniques in order to ensure reliable communication.

Besides, successful classification of the modulation order with high accuracy helps in identifying the best modulation order. In other words, the classification accuracy can be used as a forward channel quality indicator (CQI) engine to optimise the modulation order, as shown in Fig. 1(a). One important factor that can affect the transmission of data is the modulation order, which refers to the number of possible states that the carrier signal can take on. A higher modulation order allows for more data to be transmitted, but it can also make the signal more susceptible to interference. By using a CQI engine to optimize the modulation order, it is possible to improve the quality and reliability of data transmission over the forward channel. The CQI index value is based on the accuracy of detection rather than the traditional scale ranging from 0 (poorest channel quality) to 15 (best channel quality). High detection accuracy refers to better channel quality, thereby using the same or higher classified modulation order at the transmission and vice versa, as shown in Fig. 1(b). Due to the vehicular channel quality fluctuation between high and low in urban and rural areas, respectively, the modulation order must be optimised between the communicating terminals for an acceptable probability of error P_e. However, the channel's unpredictable behaviour (i.e., line-of-sight and non-line-of-sight variations) and the hardware imperfections (i.e., carrier frequency offset and the additive noise) lead to unexpected signal variations which results in increasing P_e, posing a challenging scenario. This makes the need for a reliable modulation classification technique for fast and slow fading vehicular channels crucial. The current state-of-the-art of modulation optimisation for mobile and vehicular communication depends on channel probing [5], which consumes high communication overhead. Pilot-based channel estimation schemes are characterized by a high amount of communication overhead and low spectrum utilization. In this challenging scenario, this paper contributes the following:

1) For effective observation of unoccupied channels, we apply the spectrum aggregation-based ultra-wideband spectrum monitoring method.
2) By using deep learning, this work develops a lightweight feature-based modulation classification approach that can detect modulation order with high probability of detection for an acceptable P_e.
3) Based on a 3-dimension (3D) stochastic vehicular channel, the proposed approach was evaluated at various ve-
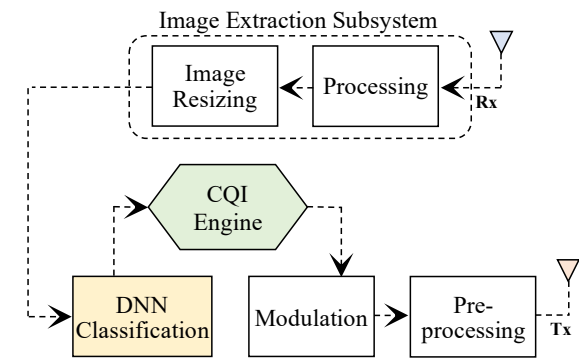
(a) Block diagram of the modulation classification.
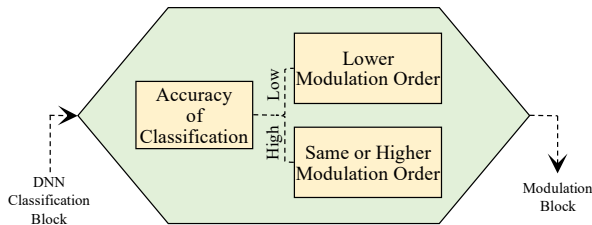
(b) CQI optimisation engine.

Fig. 1: The proposed spectrum awareness approach.

hicle speeds, signal-to-noise ratios (SNRs), and channel variations in urban and rural areas.

The paper is organised as follows. Section II introduces related works. Section III presents the 3D stochastic V2V channel model and deep learning model. Sections IV and V discuss the proposed approach and performance evaluation, respectively. Finally, Section VI concludes the paper.

II. RELATED WORKS

In this section, we review the recent works related to spectrum monitoring and modulation classification.

A. Spectrum monitoring techniques

According to the literature presented by Gupta et al. [4], two major schemes are presented for spectrum monitoring, receiver statistics-based, and energy ratio-based spectrum monitoring. The former is used to detect the presence of primary users by counting the bit error using a low-density parity check code and comparing it with a threshold value. However, the hardware impairments affects the bit error counting used for spectrum monitoring. The latter observes the spectrum at the transmitter end based on the subcarriers. For determining the energy ratio, two same-level sliding windows are used consecutively. Robert et al. [6] propose a real-time monitoring system that can gather data from a three-axis antenna on three synchronised receiving channels. Shiba et al. [7] introduce a multi-frequency sampling network for designing a wideband spectrum monitor in the internet of things applications. In this study, we use the NI-LabView example block diagram that utilizes the aggregate spectrum built up band-by-band for spectrum monitoring; see ref. [8] for more information.
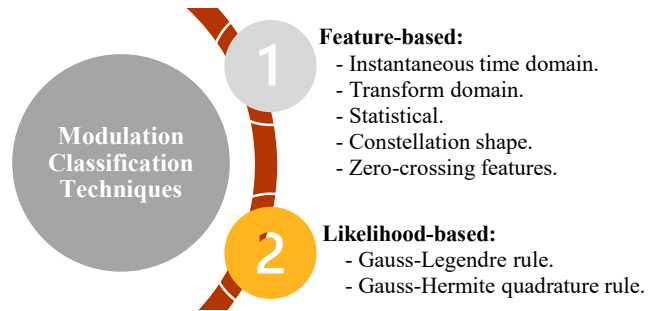

Fig. 2: Techniques for modulation classification [13]

B. Modulation classification techniques

The two major categories of modulation classification techniques are likelihood-based (LB) [9], [10] and feature-based (FB) [11], [12], see Fig. 2. The former classifies modulation as multiple hypotheses testing problems that lead to optimal solutions but are computationally complex and requires pre-known channel parameters. As for the latter, it uses features to represent the signal, and if features and classifiers are chosen properly, it can achieve nearly optimal performance with reduced complexity. To reduce the complexity of the LB technique, Shi et al. [9] propose two approximate LB algorithms to classify linearly modulated signals using Gauss–Legendre and Gauss–Hermite quadrature rules. Zheng et al. [10] introduce a maximum average likelihood algorithm for orthogonal frequency division multiplexing (OFDM) system to determine the modulation order. However, complexity has a trade-off with the total number of possible active subcarrier patterns. For FB technique, Lee et al. [11] converted the characteristic values of wireless signals into 2D images. Afterwards, signals are classified using a convolutional neural network (CNN). Nevertheless, this method is not capable of detecting all forms of signals. On the basis of the feature selection algorithm, Zhang et al. [12] present a mixed recognition algorithm. A tree-like feature structure is also used to develop a multi-layer smooth support vector machine classifier (SVM). However, most existing classification techniques only consider classification performance at different SNRs without considering variation and instability in channels [14], [15]. To the best of our knowledge, this study is unique in that it evaluates the proposed approach in urban and rural areas under different channel conditions.

III. PRELIMINARIES

This section reviews the V2V channel modeled in [16] and discusses the designed deep learning model.

A. Review of the 3D stochastic V2V channel [16]

This study adopts the stochastic vehicular channel modeled in [16]. Consider a scenario in which two vehicles, Alice and Bob, wirelessly communicate at a central frequency f_c. In this case, Bob's received signal is the combination of a number of L components coming from different moving and fixed scatterers, see Fig. 3. The lth multipath component has a different fading coefficient and phase delay denoted by a_l and
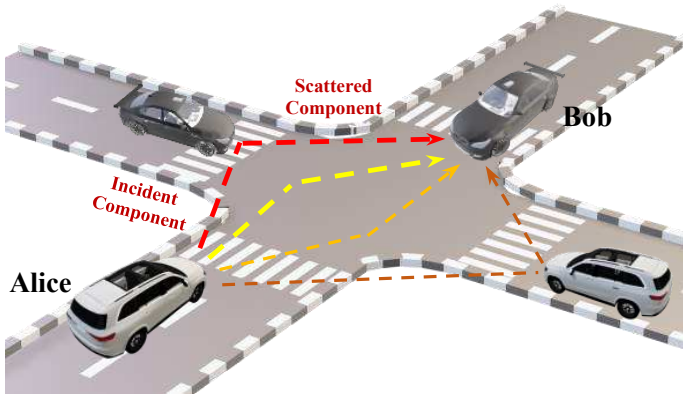
Fig. 3: Vehicular channel model representation for spectrum awareness.

TABLE I: Channel parameter settings

Channel Parameters	Value
Number of multipath components (L)	Urban: 16, Rural: 5
Speed of Tx/Rx	$10, 20, 30$ m/s
Speed of the scatterer	30 m/s
Azimuth departure/arrival angles $\left(\alpha_{A(B),l}\right)$	$U[-\pi, \pi)$
Departure/arrivals' elevation angles $\left(\beta_{A(B),l}\right)$	$U[-\pi, \pi)$
Incident reflected scatterers' angles $\left(\alpha_{1(2),l}\right)$	$U[0, \pi/3)$
Weibull distribution - scale coefficient (ρ)	2.985
Weibull distribution - shape coefficient (a)	0.428

ϕ_l, respectively. Hence, the channel observation at the side of Bob at time t is represented by

$$H_B(t) = \sum_{l=1}^{L} |a_l| \exp\left(j\phi_l\right) \exp\left(j2\pi v_l t\right) \qquad (1)$$

where the doppler parameter v_l combines Alice's, Bob's, and the l scatterer's doppler shifts, denoted by $v_{A,l}$, $v_{B,l}$, and $v_{S,l}$, respectively, as follows.

$$v_l = v_{A,l} + v_{B,l} + v_{S,l} \qquad (2)$$

where

$$v_{A(B),l} = u_{A(B)\max} \frac{f_c}{c} \cos\alpha_{A(B),l} \cos\beta_{A(B),l}$$
$$v_{S,l} = u_S \frac{f_c}{c} \left(\cos\alpha_{1,l} + \cos\alpha_{2,l}\right) \qquad (3)$$

where $u_{A(B)\max}$ is the Alice's and Bob's vehicles maximum speeds, $\alpha_{A(B),l}$ and $\beta_{A(B),l}$ are the Alice's and Bob's azimuth and elevation angles of departure and arrivals, respectively, and $\alpha_{S,l}$ and $\beta_{S,l}$ are the scatterers' incident and reflected angles, respectively. According to ref. [16], the randomness of scatterer's speed u_S follows the Weibull distribution denoted by

$$p_{u_S}(u_S) = w u_S^{a^{-1}} \exp\left(-w u_S^a / a\right) \qquad (4)$$

where w and a are scale and shape parameters, respectively. In this study, we modeled the V2V channel with parameter settings listed in Table I.
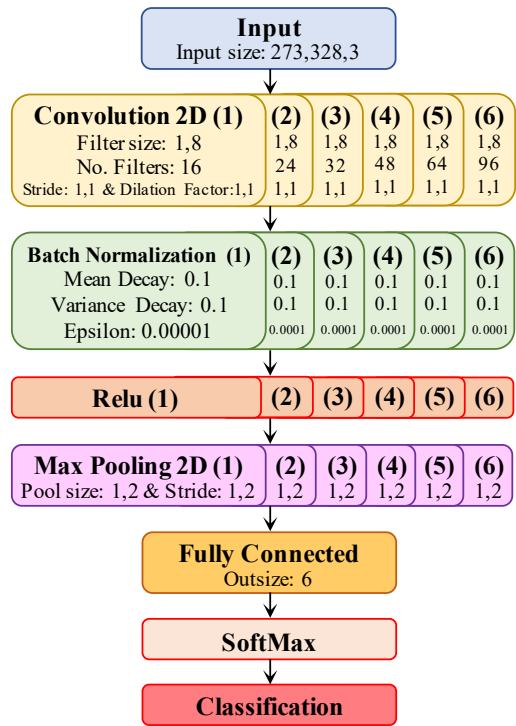

Fig. 4: The proposed deep learning model architecture.

B. The proposed image-based deep learning model

This subsection details the deep neural network (DNN) classification block highlighted in yellow in Fig. 1(a). Fig. 4 presents the flowchart of the proposed image-based deep learning model. The input layer is an RGB image layer having dimensions 273×328 pixels followed by 6 consecutive 2D convolution layers with filter numbers equal to $\{16, 24, 32, 48, 64, 96\}$. Each convolution layer is followed by batch normalization, ReLU activation, and 2D max pooling layers. The last max pooling layer is connected to a fully connected (FC) layer with 6 classes and weight and bias learn rate factors equal 10. Finally, the FC layer is followed by softmax and classification output layers. The total number of layers is 28 layers. Training the network involves tuning some of the parameters. Correctly adjusting these parameters according to constellation image data input helps create a good model in less computational time. For the training process, we use the "adam" solver, set the initial learn rate to 0.001, the validation frequency to 50, max epochs to 30, and mini-batch size to 64.

IV. SPECTRUM AWARENESS APPROACH

This section discusses the employed spectrum awareness approach, including spectrum monitoring and modulation classification techniques. For ultra-wideband spectrum monitoring, we use the NI-LabView example given in [8] and the USRP X310-1st RF channel. Then, we set the start and stop frequencies to be 5.88 to 5.91 GHz, respectively. In addition, we run the signal transmission at the 2nd channel of the USRP at $f_c = 5.9$ GHz. Fig. 5 shows the received spectrum,
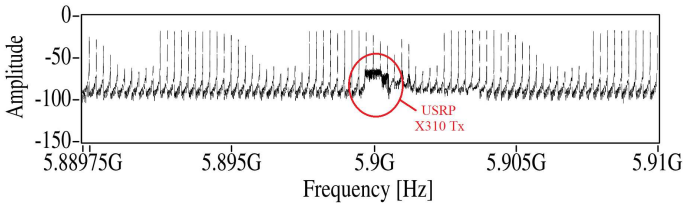
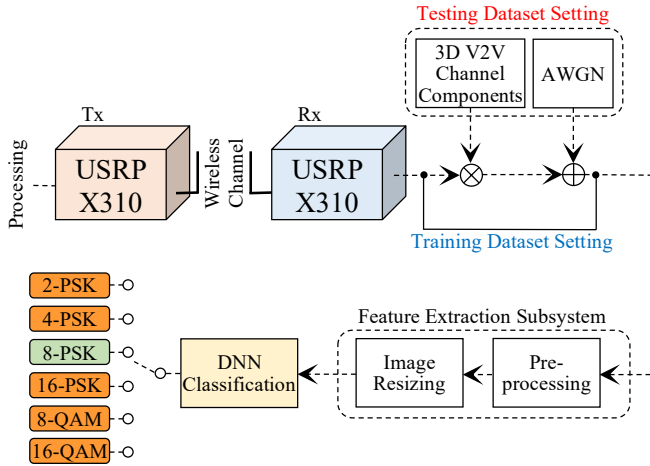Fig. 5: Spectrum monitoring from 5.88 to 5.91 GHz.

Fig. 6: Implementation block diagram.

highlighting the USRP X310 transmitter channel. It can be noted that the amplitude of the spectrum sensed at 5.9 GHz is higher than that of unoccupied channels. Then, we present the modulation classification technique in a two-phase process as follows.

A. The training phase

In this phase, the training dataset setting, depicted in Fig. 6, is adjusted for acquiring the dataset used for training the DNN. It is noteworthy to mention that the training dataset has the internal additive complex gaussian noise of the USRP X310 receiver channel. We use an OFDM communication system at $f_c = 5.9$ GHz for the DSRC, with 256 subcarriers, 64 cyclic-prefix, and 125 subcarriers holding the transmitted data. Then, we use 2-PSK, 4-PSK, 8-PSK, 16-PSK, 8-QAM, and 16-QAM modulation and demodulation processes at the side of the transmitter and receiver, respectively. According to the modulation order, we acquired 150 training images with dimensions 273×328 pixels for each constellation type. Training samples for different constellations in the polar coordinates (in-phase and quadrature axes) are presented in Fig. 7. Based on the obtained data, the total training time was [74:13] minutes using Core-i7 CPU @ 2.7 GHz laptop with 16 GB RAM.

B. The classification phase

In this phase, using the testing dataset setting depicted in Fig. 6, we simulated the 3D stochastic V2V channel reviewed in subsection III(A). Using the channel parameter settings listed in Table I and the complex additive gaussian noise block,
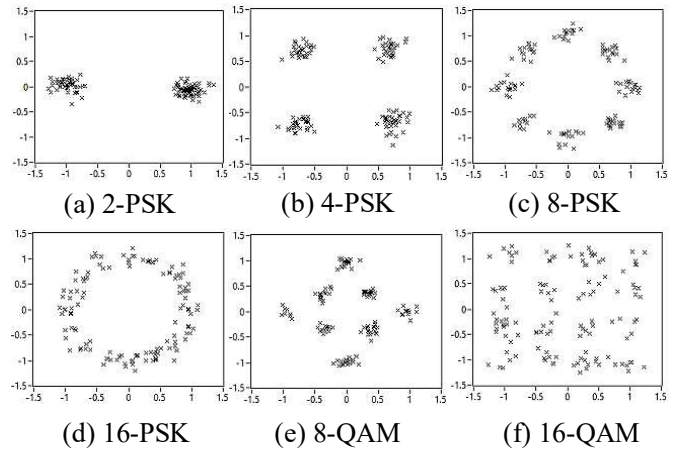

Fig. 7: Training samples of different constellations.

we evaluated the classifier's performance at different SNRs, vehicle speeds, and channel variations in urban and rural areas. For urban and rural areas, we set L to 16 and 5 multipath components, respectively. These components are convoluted with the received OFDM symbol at the receiver side. Based on the power of the added complex gaussian noise, we evaluated the probability of detection P_d at different SNRs.

V. PERFORMANCE EVALUATION

In this section, we examine how classification performance is affected under different test parameters (i.e., channel variations $var.$, speed, SNRs) in urban and rural areas. Four experiments were conducted where three parameters were kept constant while one parameter varied for each case. The following are the experiments analyses.

A. Experiment 1: P_d at different channel variations $var.$

In this experiment, we set the maximum vehicle speeds $u_{A(B)_{\max}}$ in (3) to 30 m/s and SNR value to 25 dB simulated in an urban area (i.e, L equals 16 multipath components). Then, we adjusted the value of the channel variation $var.$ to 0.1, 0.3, and 0.6. Table II shows P_d of the six modulation constellations at the mentioned $var.$ values. It can be noted that P_d is inversely proportional to the increase in the $var.$ value. For example, for 8-PSK, the P_d equals 90.1% at $var. = 0.1$. While this value at $var. = 0.3$ and 0.6 are 87.1% and 86.5%, respectively. The reason for this fact is that the increment in the $var.$ value results in higher scattered constellations, leading to lower P_d. According to the 16-QAM constellation, the P_d is not affected by the $var.$ as it has unique constellation points compared to other classes.

B. Experiment 2: P_d at different vehicle speeds $u_{A(B)_{\max}}$

In this experiment, we set the channel variation $var.$ to 0.3 and SNR value to 25 dB simulated in an urban area. Then, we adjusted the value of $u_{A(B)_{\max}}$ to 10, 20, and 30 m/s. Table III shows P_d of the six modulation constellations at different vehicle speeds. It can be noted that P_d is inversely proportional to the increase in the $u_{A(B)_{\max}}$ value. For example, for 8-PSK, the P_d equals 89.1% at $u_{A(B)_{\max}} = 10$ m/s. While this

TABLE II: P_d at different channel variations

Modulation order	SNR = 25 dB, Speed = 30 m/s, Urban		
	$var. = 0.1$	$var. = 0.3$	$var. = 0.6$
2-PSK	76.9%	76.2%	72.7%
4-PSK	98.7%	98.6%	98.1%
8-PSK	90.1%	87.1%	86.5%
16-PSK	87.5%	86.5%	85.9%
8-QAM	79.3%	78.7%	77.3%
16-QAM	100%	100%	100%

TABLE III: P_d at different vehicle speeds

Modulation order	SNR = 25 dB, $var. = 0.3$, Urban		
	Speed = 10 m/s	Speed = 20 m/s	Speed = 30 m/s
2-PSK	77.8%	76.9%	76.2%
4-PSK	98.9%	98.9%	98.6%
8-PSK	89.1%	88.6%	87.1%
16-PSK	88.7%	88.1%	86.5%
8-QAM	81.5%	79.5%	78.7%
16-QAM	100%	100%	100%

TABLE IV: P_d at different signal-to-noise ratios

Modulation order	Speed= 30 m/s, $var. = 0.3$, Urban		
	SNR = 15 dB	SNR = 20 dB	SNR = 25 dB
2-PSK	68.3%	72.4%	76.2%
4-PSK	91.7%	97.7%	98.6%
8-PSK	82.3%	84.5%	87.1%
16-PSK	84.9%	85.7%	86.5%
8-QAM	73.4%	74.7%	78.7%
16-QAM	100%	100%	100%

TABLE V: P_d in urban and rural areas

Modulation order	Speed= 30 m/s, $var. = 0.3$, SNR = 25 dB	
	Urban	Rural
2-PSK	76.2%	99.1%
4-PSK	98.6%	100%
8-PSK	87.1%	98.5%
16-PSK	86.5%	100%
8-QAM	78.7%	97.9%
16-QAM	100%	100%

TABLE VI: The confusion matrix at Speed= 30 m/s, $var. = 0.3$, and SNR = 25 dB in urban area

True	2-PSK	4-PSK	8-PSK	16-PSK	8-QAM	16-QAM
2-PSK	76.2	0	0	0	23.8	0
4-PSK	0	98.6	0	0	0	1.4
8-PSK	0	0	87.1	12.8	0	0.01
16-PSK	0	0	0.3	86.5	0	13.2
8-QAM	0	0	1.3	9.2	78.7	1.8
16-QAM	0	0	0	0	0	100
	2-PSK	4-PSK	8-PSK	16 -PSK	8-QAM	16-QAM
	Probability of detection (%)					

value at $u_{A(B)_{\max}} = 20$ and 30 m/s are 88.6% and 87.1%, respectively.

C. Experiment 3: P_d at different SNRs

In this experiment, we set the channel variation $var.$ to 0.3 and $u_{A(B)_{\max}}$ in (3) to 30 m/s simulated in an urban area. Then, we adjusted the value of the SNR to 15, 20, and 25 dB. Table IV shows P_d of the six modulation constellations at different SNRs. It can be noted that P_d is directly proportional to the increase in the SNR. For example, for 8-PSK, the P_d equals 87.1% at SNR = 25 dB. While this value at SNR = 20 and 15 dB are 84.5% and 82.3%, respectively.

D. Experiment 4: P_d in urban and rural areas

In this experiment, we set the channel variation $var.$ to 0.3, $u_{A(B)_{\max}}$ in (3) to 30 m/s, and SNR to 25 dB. Then, we adjusted the value of the L in (1) to 16 and 5 multipath components for urban and rural areas, respectively. Table V shows P_d of the six modulation constellations in both scenarios. It can be noted that P_d in a rural area is better than that of an urban area. For example, for 8-PSK, the P_d equals 98.5% in a rural area. While this value equals 87.1% in an urban area.

Finally, we summarise a case experiment in the form of a confusion matrix, as presented in Table VI. These results are obtained at $var. = 0.3$, $u_{A(B)_{\max}} = 30$ m/s, and SNR = 25 dB simulated in an urban area. As shown in the matrix, there are two major confusing cases. In case 1, the network confuses 2-PSK with 8-QAM, which only happens at low SNRs and high $u_{A(B)_{\max}}$ and $var.$. In case 2, the network confuses 16-PSK with 16 QAM due to the same reasons discussed in case 1, leading to false detection probability.

VI. CONCLUSIONS

This paper introduces an efficient deep learning-based modulation optimisation order that saves significant communica-

tion overhead compared to channel probing-based approaches. By designing a CQI engine block, we optimise the modulation order for V2V channel. The evaluation process discussed the effects of the channel variations, vehicle speeds, and SNR values on the classifier's detection probability in urban and rural areas. Based on the experimental results, the proposed classifier has sufficient detection probability for an acceptable false detection $\leq 20\%$. In future work, we will explore the possibility of testing the classifier on a realistic vehicular wireless channel at varying terminal speeds.

REFERENCES

[1] M. A. Al-Shareeda, M. Anbar, and I. Hasbullah, "Survey of Authentication and Privacy Schemes in Vehicular Ad Hoc Networks", *IEEE Sensors Journal*, vol. 21, no. 2, Jan. 2021.

[2] M. A. Shawky, Q. H. Abbasi, M. A. Imran, S. Ansari, and A. Taha, "Cross-Layer Authentication based on Physical-Layer Signatures for Secure Vehicular Communication", IEEE Intelligent Vehicles Symposium (IV), pp. 1315-1320, 2022.

[3] G. Wu, and H. Chu, "Spectrum Sharing with Vehicular Communication in Cognitive Small-Cell Networks", *International Journal of Antennas and Propagation*, vol. 2020, Mar. 2020.

[4] M. S. Gupta, K. Kumar, "Progression on spectrum sensing for cognitive radio networks: A survey, classification, challenges and future research issues", Journal of Network and Computer Applications, vol. 143, pp. 47-76, 2019.

[5] C. MehlfQihrer, M. Wrulich, J.C. Ikuno, D. Bosanska, and M. Rupp, "Simulating the Long Term Evolution physical layer", in Proc. of 17th European Signal Processing Conference (EUSIPCO 2009) Glasgow, Scotland, UK, pp. 1471-1478, 2009.

[6] H. Robert, B. Paul, M. Simona, and S. Annamaria, "Real Time Broadband Electromagnetic Spectrum Monitoring System based on Software Defined Radio Technology", 9_{th} International Conference on Modern Power Systems (MPS), pp. 1-6, 2021.

[7] T. Shiba, T. Furuichi, K. Akimoto, M. Motoyoshi, S. Kameda, and N. Suematsu, "Real-Time Wideband Spectrum Monitor Using Multiple Sampling Frequency Direct RF Undersampling for Wireless IoT", 2021 51st European Microwave Conference (EuMC), pp. 725-728, 2022.

[8] NI, "Wideband Spectrum Monitoring with NI USRP", available at: https://forums.ni.com/t5/Example-Code/Wideband-Spectrum-Monitoring-with-NI-USRP/ta-p/3533000.

[9] Q. Shi, and Y. Karasawa, "Automatic modulation identification based on the probability density function of signal phase", *IEEE Trans. Commun.*, vol. 60, no. 4, pp. 1033–1044, Apr. 2012.

[10] J. Zheng, and Y. Lv, "Likelihood-Based Automatic Modulation Classification in OFDM With Index Modulation", *IEEE Trans. on Vehicular Tech.*, vol. 67, no. 9, pp. 8192-8204, Sep. 2018.

[11] J. H. Lee, K. -Y. Kim and Y. Shin, "Feature Image-Based Automatic Modulation Classification Method Using CNN Algorithm", 2019 International Conference on Artificial Intelligence in Information and Communication (ICAIIC), pp. 1-4, 2019.

[12] X. Zhang, J. Sun, and X. Zhang, "Automatic Modulation Classification Based on Novel Feature Extraction Algorithms", *IEEE Access*, vol. 8, pp. 16362-16371, 2020.

[13] S. Peng, S. Sun, and Y. -D. Yao, "A Survey of Modulation Classification Using Deep Learning: Signal Representation and Data Preprocessing," *IEEE Transactions on Neural Networks and Learning Systems*, pp. 1 - 19, Jun. 2021.

[14] N. Daldal, A. Sengur, K. Polat, and Z. Cömert, "A novel demodulation system for base band digital modulation signals based on the deep long short-term memory model", *Appl. Acoust.*, vol. 166, no. 107346, Sep. 2020.

[15] Z. Wu, S. Zhou, Z. Yin, B. Ma, and Z. Yang, "Robust Automatic Modulation Classification Under Varying Noise Conditions", *IEEE Access*, vol. 5, pp. 19733-19741, 2017

[16] P. Karadimas, and D. Matolak, "Generic stochastic modeling of vehicle-to-vehicle wireless channels", *Vehicular Communications*, vol. 1, no. 4, pp. 153–167, 2014.